Influence of Alkyl Substitution Position on Wide-Bandgap Polymers in High-Efficiency Nonfullerene Polymer Solar Cells

Qing Guo[#], Wanbin Li[#], Guangda Li, Kun Wang*, Xia Guo*, Maojie Zhang*, Yongfang Li, Wai-Yeung Wong*

Q. Guo, W. B. Li, G. D. Li, Prof. X. Guo, Prof. M. J. Zhang, Prof. Y. F. Li
Laboratory of Advanced Optoelectronic Materials, College of Chemistry, Chemical Engineering and Materials Science, Soochow University, Suzhou 215123, China.
E-mail: guoxia@suda.edu.cn; mjzhang@suda.edu.cn
Dr. K. Wang
School of Materials and Chemical Engineering, Zhongyuan University of Technology, Zhengzhou 451191, China.
E-mail: kwang@zut.ed.cn
Prof. W.-Y. Wong
Department of Applied Biology and Chemical Technology, The Hong Kong Polytechnic University, Hung Hom, Hong Kong, China
E-mail: wai-yeung.wong@polyu.edu.hk
Prof. W.-Y. Wong
The Hong Kong Polytechnic University Shenzhen Research Institute, Shenzhen 518057, China

[#] These authors contributed equally to this work.

Keywords: non-fullerene polymer solar cells; substitution position; alkyl side chain; benzodithiophene-4,8-dione; wide bandgap polymer

Abstract:

Two wide-bandgap (WBG) conjugated polymers (PBPD-*p* and PBPD-*m*) based on phenyl-substituted benzodithiophene (BDT) with the different substitution position of the alkyl side chain and benzodithiophene-4,8-dione (BDD) units were designed and synthesized to investigate the influence of alkyl substitution position on the photovoltaic performance of polymers in nonfullerene polymer solar cells (PSCs). The thermogravimetric analysis, absorption spectroscopy, molecular

energy level, X-ray diffraction, charge transport and photovoltaic performance of the polymers were systematically studied. Compared with PBPD-*p*, PBPD-*m* exhibited a slight blue-shift but a deeper highest occupied molecular orbital (HOMO) energy level, a stronger (100) diffraction peak with tighter alkyl chain packing and a higher hole mobility. The PBPD-*m*-based PSCs blended with acceptor IT-4F showed a higher power conversion efficiency (PCE) of 11.95% with a high open-circuit voltage (V_{oc}) of 0.88 V, a short-circuit current density (J_{sc}) of 19.76 mA cm^{-2} and a fill factor (FF) of 68.7% when compared with the PCE of 6.97% with a V_{oc} of 0.81 V, a J_{sc} of 15.97 mA cm^{-2} and an FF of 53.9% for PBPD-*p*. These results suggest that it is a feasible and effective strategy to optimize the photovoltaic properties of WBG polymers by changing the substitution position of alkyl side chain in non-fullerene PSCs.

Introduction

Recently, nonfullerene polymer solar cells (PSCs) based on conjugated polymer donors and nonfullerene acceptors (NFAs) have been of great interest. This is because of their advantages such as easy synthesis, strong absorption in a visible region, easily tunable energy levels, and good stability[1-7], and the power conversion efficiencies (PCEs) achieved can be up to 16%[8-19]. Excellent narrow bandgap NFAs such as ITIC, IDIC, IT-4F, and IT-M have recently been shown to exhibit strong absorption in the range of 600-800 nm.[20-21] To completely utilize sunlight, the efficient wide bandgap (WBG) conjugated polymer donors must be designed and developed.

The rational design and synthesis of conjugated polymers by optimizing backbone structures for PSCs have attracted great attention and made remarkable progress.[22-28] Side-chain engineering is another important strategy to optimize structures of polymers and improve the photovoltaic performance of PSCs.[29-34] Alkyl side chain was introduced into two-dimensional conjugated side chains of the conjugated polymers, which adjusted the solubility, optical absorption, and molecular energy levels of the polymers and tuned the molecular packing and blend film morphologies of the active layer.[35-37] Several efforts are focused on the length, branching position of the alkyl chain, and type of alkyl side chains, which affect the performance of the polymers.[38-43] For example, Bin *et al.*

reported two WBG polymers (J60 and J61). Devices based on J61 showed the higher PCE of 9.53% when compared with the devices based on J60 with the PCE of 8.97% using the simple tuning of alkyl side chain length.[44] In our recent study, [43] devices based on PSBZ, which included branched 2-butyloctylthio side chains showed the higher PCE of 10.5% with the high short-circuit current density (J_{sc}) of 19.0 mA cm^{-2} when compared with the PCE of 9.53% with the J_{sc} of 17.43 mAcm^{-2} for J61, which included linear dodecylthio side chains. However, few studies are focused on the influence of a side-chain position on the performance of J60 and J61 polymers.[45,46] For instance, two polymers (P2 and P3) with different alkyl-substitution positions on a thienyl-conjugated side chain in a benzodithiophene (BDT) unit were synthesized, and the devices based on P2 showed a higher PCE than that of P3 in fullerene-based PSCs.[45] Therefore, it is necessary to investigate the effect of alkyl substitution positions of polymers to optimize properties of the materials.

In the past few years, WBG polymers have shown great potential and advantages during the use of nonfullerene-based photovoltaic devices, which are benefited from the complementary absorption, matching energy levels, and highly balanced electron-hole mobility between a WBG polymer donor and a nonfullerene acceptor.[8-17] Huo *et al.* developed an efficient copolymer (PBDT-T1) based on BDT and benzodithiophene-4,8-dione (BDD) units, serving as a donor in PSCs, and the devices showed a PCE of 8.12% with a open-circuit voltage (V_{oc}) of 0.86 V, a J_{sc} of 13.13 mA cm^{-2} and a fill factor (FF) of 71.8%.[47] To further explore the effects of alkyl substitution position on photovoltaic properties, we designed and synthesized two WBG conjugated polymers (PBPD-*p* and PBPD-*m*) based on phenyl-substituted BDT units with different substitution positions of an alkyl side chain and BDD units. The influence of the alkyl substitution positions of the two polymers on the thermogravimetric analysis, absorption spectroscopy, molecular energy level, X-ray diffraction, charge transport, and photovoltaic performance were systematically studied. The PBPD-*m* polymer showed a slight blue-shift with a lower-lying highest occupied molecular orbital (HOMO) energy level when compared with the PBPD-*p* polymer. Moreover, the PBPD-*m* demonstrated a stronger (100) diffraction peak with a tighter alkyl chain packing and higher hole mobility (μ_h) compared

with the PBPD-*P* polymer. Nonfullerene PSCs based on the abovementioned polymers and IT-4F were fabricated. The PBPD-*m*-based devices showed a higher PCE of 11.95% with a V_{oc} of 0.88 V, a J_{sc} of 19.76 mA cm^{-2} and an FF of 68.7% compared with the PCE of 6.97% with a V_{oc} of 0.81 V, a J_{sc} of 15.97 mA cm^{-2} and an FF of 53.9% for the PBPD-*p*-based devices. These results suggest that it is a feasible and effective strategy to optimize photovoltaic properties of WBG polymers by changing the substitution position of alkyl side chain in nonfullerene PSCs.

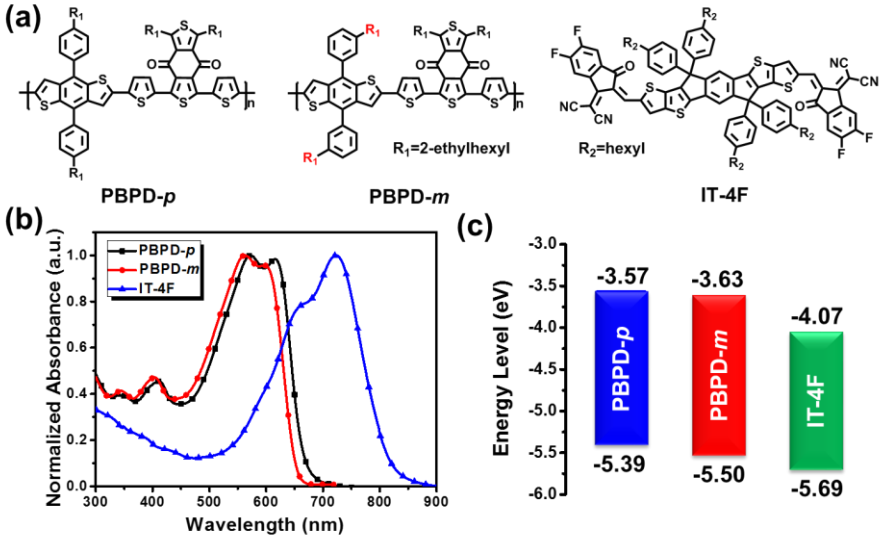

Figure 1. (a) Molecular structures; (b) absorption spectra and (c) energy level diagram of PBPD-*p*, PBPD-*m* and IT-4F.

Results and Discussion

Figure 1a shows molecular structures of PBPD-*p*, PBPD-*m*, and IT-4F polymers. The two polymers were synthesized through a Stille coupling reaction using a Pd catalyst. Synthetic routes of PBPD-*p* and PBPD-*m* are shown in Scheme S1 in the supporting information (SI). The PBPD-*m* exhibited the higher average molecular weight (M_n) of 42.1 kDa and the polydispersity index (PDI) of 2.40 than PBPD-*p* with the M_n of 22.5 kDa and the PDI of 2.38, which were measured by high-temperature gel permeation chromatography. The two polymers exhibit good solubility in common solvents such as chloroform, chlorobenzene (CB), and *o*-dichlorobenzene. The decomposition temperatures (T_d, 5% weight loss) of the PBPD-*p* and PBPD-*m* polymers were found to be 351 °C and 368 °C, respectively, as measured using the thermogravimetric analysis under an inert

atmosphere (see Figure S1a, SI), which indicates an excellent thermal stability. Differential scanning calorimetry measurement showed that there were no obvious exothermic or endothermic peaks between 30 °C and 300 °C (see Figure S1b, SI).

UV-vis absorption spectra of the two polymers in dilute CB solution and thin films were investigated (Figure S2a in the SI and Figure 1b). Table 1 contains the corresponding parameters. In the dilute solution and thin film, both the polymers showed two obvious absorption bands in the ranges of 350−450 and 500−700 nm. The maximum absorption peak of the thin films was at 572 and 563 nm for PBPD-*p* and PBPD-*m*, respectively. Both the polymers showed distinct shoulder peaks at the long-wavelength range, indicating strong intermolecular interaction in the solid film. Absorption spectra of the PBPD-*m* polymer show obvious blue-shifts both in the solution and thin film when compared with PBPD-*p*. These results may be attributed to the weaker conjugative effect of the meta-substituted alkyl group compared with the para-substituted alkyl group. The absorption edges (λ_{edge}) of PBPD-*p* and PBPD-*m* films were observed at 682 and 662 nm, which corresponded to the optical bandgap (E_g^{opt}) of 1.82 and 1.87 eV, respectively. Molecular energy levels of the two polymers were measured by electrochemical cyclic voltammetry. As shown in Figure S2(b), the onset oxidation potentials (φ_{ox}) were 0.68 and 0.79 V for the PBPD-*p* and PBPD-*m* *vs* Ag/Ag^+, respectively. The HOMO energy level (E_{HOMO}) and the lowest unoccupied molecular orbital energy level (E_{LUMO}) were calculated to be −5.39/−3.57 eV for PBPD-*p* and −5.50/−3.63 eV for PBPD-*m*, according to the equations,[48-50] $E_{HOMO} = -(E_{ox} + 4.71)$ and $E_{LUMO} = E_{HOMO} + E_g^{opt}$ eV. These results indicate that PBPD-*m* possesses deeper HOMO energy level, which enables PBPD-*m* to give higher V_{oc} in the PSCs.

Table 1. Optical properties and energy levels of the two polymers.

Polymers	λ_{max} (film) (nm)	λ_{onset} (film) (nm)	E_g^{opt} (eV)	HOMO[a] (eV)	LUMO[b] (eV)
PBPD-*p*	616	682	1.82	−5.39	−3.57
PBPD-*m*	598	662	1.87	−5.50	−3.63

[(a)] calculated using the cyclic voltammograms, [(b)] deduced from HOMO level and E_g^{opt}.

The crystallinity of the two polymers was studied by X-ray diffraction measurement, as shown in Figure 2a. The films of the PBPD-*p* and PBPD-*m* polymers showed obvious (100) diffraction peaks at 2θ= 4.3° and 5.4°, derived from the alkyl chain packing with the *d*-spacing of 20.5 Å and 16.3 Å, respectively. Furthermore, both polymers exhibited weak but clear (010) diffraction peaks at 2θ = 24.0°, obtained from the π-π stacking with the *d*-spacing of ~3.7 Å. Compared with PBPD-*p*, PBPD-*m* exhibited the stronger (100) diffraction peak and smaller *d*-spacing of alkyl chain packing, indicating the enhanced crystallinity of PBPD-*m*. Additionally, the μ_h of PBPD-*m* (1.37×10^{-3} $cm^2V^{-1}s^{-1}$) is higher than that of PBPD-*p* (1.21×10^{-3} $cm^2V^{-1}s^{-1}$) as measured by the space-charge limited current (SCLC) method (see Figure S3 and Table S1).

To investigate and compare the photovoltaic properties of PBPD-*p* and PBPD-*m* in nonfullerene PSCs, we fabricated the devices with the inverted structure of ITO/ZnO/PFN/polymer: IT-4F/MoO_3/Al and the active layers were spin-coated from CB solution. Firstly, we optimize the donor/acceptor (D/A) weight ratios of the blend film. As shown in Figure S4 and Table S2, the optimized *D*/*A* ratios were found to be 1:1 for PBPD-*p* and 1:1.5 for PBPD-*m*, respectively. The PSCs based on PBPD-*p*:IT-4F (1:1, *w*/*w*) showed the PCE of 5.83% with the V_{oc} of 0.82 V, the J_{sc} of 13.71 $mAcm^{-2}$ and the FF of 51.9%. Meanwhile, the devices based on PBPD-*m*:IT-4F (1:1.5, *w*/*w*) show the high PCE of 10.39% with the high V_{oc} of 0.89 V, theJ_{sc} of 18.13 $mAcm^{-2}$, and the FF of 64.4%. To optimize the active layer morphology and improve the photovoltaic properties, we selected the 1,8-diiodooctane (DIO) as the additive solvent. We optimized the DIO content (0.5%–1%, *v*/*v*) at the optimal D/A conditions (see Figure S5 and Table S3). By adding the DIO, we observed that the devices show increased J_{sc} and FF. It is clear that both polymers showed the best performance when 0.75% DIO was added. Figure 2 shows the current−density voltage (*J*−*V*) curves of the devices. Table 2 summarizes the corresponding photovoltaic parameters. The devices based on PBPD-*p*:IT-4F blend film with 0.75% DIO showed the PCE of 6.97% with the V_{oc} of 0.81 V, the J_{sc} of 15.97 $mAcm^{-2}$, and the FF of 53.9%. Meanwhile, the devices based on PBPD-*m*:IT-4F showed the higher PCE of 11.95% with the high V_{oc} of 0.88 V, the J_{sc} of 19.76 $mAcm^{-2}$, and the FF

of 68.7%. The higher V_{oc}, J_{sc}, and the FF of PBPD-*m*-based devices are consistent with its deeper HOMO energy level and higher μ_h. The high J_{sc} values of the devices can also be confirmed from the external quantum efficiency (EQE) spectra as shown in Figure 2c. All devices display a broad photoresponse in the range from 300 to 800 nm. For the polymers IT-4F-based devices, the maximum EQE values reached 64.2% for PBPD-*p* and 77.3% for PBPD-*m*. Moreover, the EQE values of the PBPD-*m*: IT-4F devices are higher than those of the devices based on PBPD-*p*: IT-4F in the range from 300 to 800 nm, matching well with its higher J_{sc} values. The integral J_{sc} calculated from the EQE curves is consistent with the measured values from the *J*-*V* tests with the deviation of less than 5%.

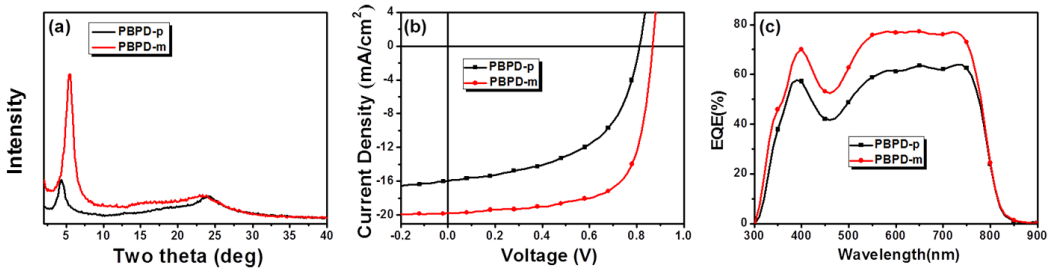

Figure 2. (a) X-ray diffration patterns of PBPD-*p* and PBPD-*m* films casted from CB on Si substrates. (b) the *J*−*V* curves; (c) EQE curves of the PSCs based on polymers:IT-4F with 0.75% DIO additive under the illumination of AM 1.5G, 100 mW cm^{-2}.

Table 2 Photovoltaic performances of the PSCs based on polymer:IT-4F with 0.75% DIO additive under the illumination of AM1.5G (100 mW cm^{-2}).

Polymer	D/A (w/w)	V_{oc} (V)	J_{sc}[a)] (mA cm^{-2})	*FF* (%)	PCE[b)] (%)
PBPD-*p*	1:1	0.81	15.97 (15.41)	53.9	6.97 (6.93)
PBPD-*m*	1:1.5	0.88	19.76 (18.87)	68.7	11.95 (11.88)

a) values calculated from EQE in brackets. [b)] average PCEs in brackets for 20 devices.

We synthesized batches of polymer donors PBPD-*m* with different molecular weights to investigate the effect of the molecular weight on the performance of the device based on PBPD-*m*.

We obtained that the polymer sample with the M_n of 24.2 kDa and the PDI of 2.22 exhibits the PCE of 11.5% with the V_{oc} of 0.89 V, the J_{sc} of 19.21 mAcm^{-2}, and the FF of 67.3%. In contrast, we observed that the polymer sample with the M_n of 42.1 kDa and the PDI of 2.40 exhibits the PCE of 11.95% with the V_{oc} of 0.88 V, the J_{sc} of 19.76 mAcm^{-2}, and the FF of 68.7%. We obtained that the polymer solar cells based on PBPD-*m* with different molecular weights show almost similar photovoltaic parameters.

The hole and electron mobilities (μ_e) were measured to understand the influence of alkyl substitution position on the device performance by using the SCLC method. As shown in Figure S3 and Table S1 (SI), for the blend films at the optimal conditions, the devices based on PBPD-*m*:IT-4F showed the μ_h of 5.63 × 10^{-4} cm^{2}V^{-1}s^{-1} and the μ_e of 3.49 × 10^{-4} cm^{2}V^{-1}s^{-1} compared with the μ_h of 3.04 × 10^4 cm^{2}V^{-1}s^{-1} and theμ_e of 9.74 × 10^5 cm^{2}V^{-1}s^{-1} of PBPD-*p*:IT-4F-based devices. Therefore, the higher and more balanced mobilities of PBPD-*m*:IT-4F blend film is beneficial to obtain higher J_{sc} and FF in the devices.

The influence of alkyl substitution position on the exciton dissociation and charge collection process in PSCs was investigated by measuring the dependence of the photocurrent density (J_{ph}) *vs* effective voltage (V_{eff}).[51] For the devices based on polymers:IT-4F, all the photogenerated excitons are dissociated into free carriers and collected by the electrodes when J_{ph} reaches saturation (J_{sat}) at large V_{eff} ($V_{eff} \geq 2$ V). The exciton dissociation probability ($P(E, T)$) can be estimated using the value of the J_{ph}/J_{sat} ratio. As shown in Figure 3a, under short-circuit conditions, the J_{ph}/J_{sat} ratios were 86.8% for the PBPD-*p* and 92.8% for PBPD-*m* polymers at optimal conditions. The results imply that the meta-position substitution of the alkyl chains in the phenyl-substituted BDT unit is beneficial for efficient exciton dissociation and charge collection efficiency in this system, corresponding to the increased J_{sc}. The dependence of V_{oc} and J_{ph} under different light intensities (P_{light}) was measured to investigate the charge recombination mechanism as shown in Figure 3b. The slope of V_{oc} *vs* log(P_{light}) can be used to estimate the degree of trap-assisted or bimolecular recombination. In general, the trap-assisted recombination is dominant when the slope is equal to 2

kT/*q*. Meanwhile, the slope of 1 *kT*/*q* suggests that the bimolecular recombination is dominant.[52] In this study, the devices based on polymers:IT-4F at the optimal conditions show slopes of 1.23 and 1.08 *kT*/*q* for the PBPD-*p* and PBPD-*m* polymers, respectively. This indicates that the bimolecular recombination is dominant in the devices based on two polymers. The meta-position substitution of the alkyl chains in this system could reduce the trap-assisted recombination and produce high J_{sc}. Figure 3c shows the relationship between J_{ph} and P_{light} (can be described by $J_{ph} \propto (P_{light})^{S}$), where *S* represents the extent of the bimolecular recombination. The slope *S*-value close to 1 indicates weak bimolecular recombination in the device.[53] In this study, we found that the devices based on the PBPD-*p*:IT-4F exhibit the *S*-value of 0.93 while the *S*-value of 0.98 was obtained for the devices based on the PBPD-*m*:IT-4F, revealing that the meta-position substitution of alkyl chains could effectively reduce bimolecular recombination.

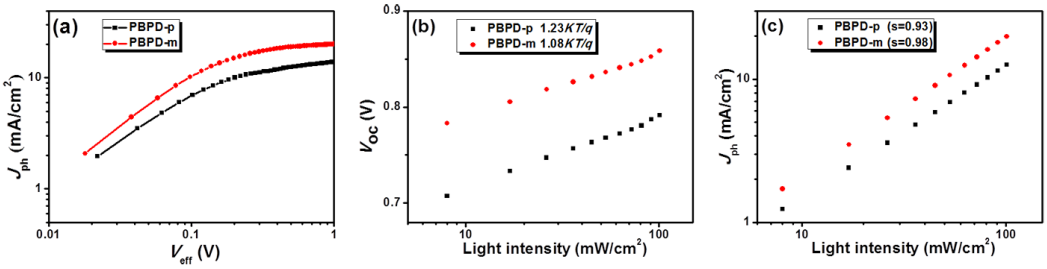

Figure 3. (a) J_{ph} versus V_{eff} characteristics, and dependence of V_{oc} (b) and J_{ph} (c) on light intensity for the PSCs based on polymers:IT-4F with 0.75% DIO additive.

We measured the photoluminescence (PL) spectra of the polymers, IT-4F, and related blends to investigate a photo-induced electron transfer behavior between the polymers and IT-4F. As shown in Figure 4, compared with the pure polymer, the fluorescence quenching efficiency of PBPD-*m*:IT-4F blend film is 95.3% while that of the PBPD-*p*:IT-4F blend film is 87.6% under the same conditions. Meanwhile, compared with the PL spectra of the pure IT-4F, the fluorescence quenching efficiency of the blend film is 90.3% and 94.5% for PBPD-*p* and PBPD-*m*, respectively. Higher fluorescence quenching efficiency of the device based on PBPD-*m*:IT-4F indicates effective

photo-induced charge transfer between PBPD-*m* and IT-4F, which is consistent with the higher J_{sc} and EQE values of the device.

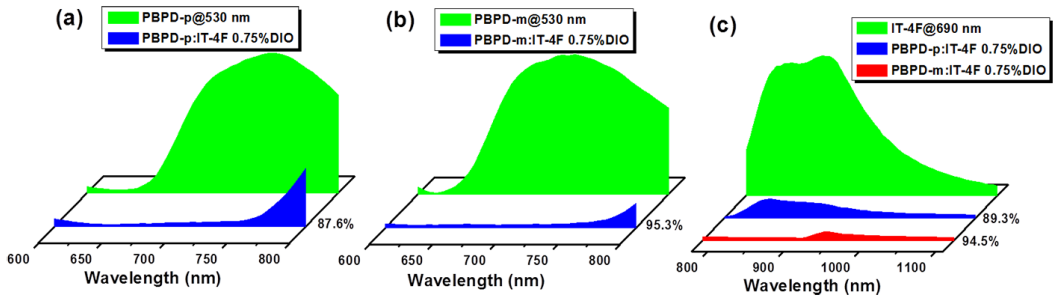

Figure 4. The PL spectra of the polymers and IT-4F with the related blend films. (a) excited at 530 nm for PBPD-*p* and the related blend films, (b) excited at 530 nm for PBPD-*m* and the related blend films, (c) excited at 690 nm for IT-4F and the related blend films.

We used atomic force microscopy (AFM) and transmission electron microscopy (TEM) to study the surface and bulk morphology of the active layers. Figure 5 shows AFM and TEM images based on the blend film with 0.75% DIO additive. For the AFM images, the root-mean-square values are 4.96 and 1.53 nm for the blend films based on the PBPD-*p* and PBPD-*m* polymers, respectively. This indicates the smoother surface and improved miscibility of the PBPD-*m*-IT-4F blend films. For the TEM images, large domains are emerged in the PBPD-*p*:IT-4F film. Meanwhile, the blend film based on the PBPD-*m* and IT-4F polymers shows obvious fibrillar structure and nanoscale phase separation beneficial for charge separation and transport and achieving higher J_{sc} and FF.

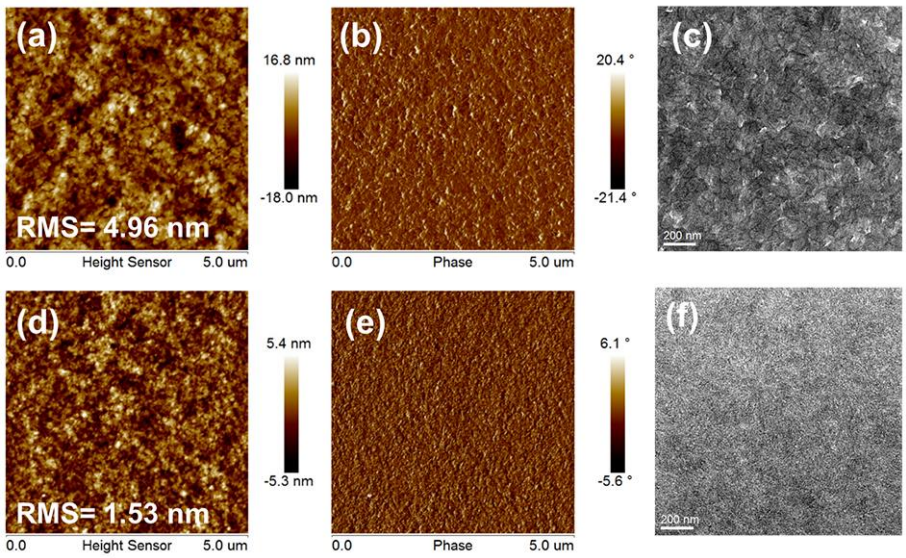

Figure 5. The AFM and TEM images of the polymer:IT-4F blend films in the optimal conditions: (a), (b) and (c) for PBPD-*p*:IT-4F, and (d), (e) and (f) for PBPD-*m*: IT-4F.

In conclusion, we designed and synthesized two WBG conjugated polymers (PBPD-*p* and PBPD-*m*) based on phenyl-substituted BDT with different substitution positions of the alkyl side chain and BDD units. The influence of the alkyl substitution position on the photovoltaic performance of the polymers in PSCs was investigated. Compared with the PBPD-*p* polymer, the PBPD-*m* polymer exhibited a deeper HOMO energy level, a tighter alkyl chain packing, and a higher μ_h. In combination with IT-4F, the devices based on PBPD-*m* polymer showed the higher PCE of 11.95% with the high V_{oc} of 0.88 V, the J_{sc} of 19.76 mA cm^{-2}, and the FF of 68.7%, while the PBPD-*p*-based device showed a relatively weak photovoltaic performance. These results suggest that it is a feasible and effective strategy to optimize photovoltaic properties of the WBG polymers by changing the substitution position of alkyl side chain in nonfullerene PSCs.

Supporting Information

Supporting Information is available from the Wiley Online Library or from the author.

Acknowledgements

Q. Guo and W. B. Li contributed equally to this work. This work was supported by National Natural Science Foundation of China (NSFC) (No. 51573120, 51773142, 51873176 and 51973146), Jiangsu Provincial Natural Science Foundation (Grant No. BK20190099), Collaborative Innovation Center of Suzhou Nano Science & Technology, the Priority Academic Program Development of Jiangsu Higher Education Institutions. W.-Y.W. acknowledges the financial support from the Science, Technology and Innovation Committee of Shenzhen Municipality (JCYJ20180507183413211), Hong Kong Research Grants Council (PolyU123384116P), the Hong Kong Polytechnic University (1-ZEIC) and Ms. Clarea Au for the Endowed Professorship in Energy (847S). This work was also supported by the Science and Technology Innovative Talents in Universities of Henan Province (20HASTIT030), Henan Province Science and Technology Planning Project (182102210530), the Training Plan of Young Backbone Teachers in Colleges and Uiversities of Henan Province (2019GGJS141), Key Scientific Research Projects of Higher Education Institutions of Henan Province (20B150032), Science and technology guidance program of China Textile Industry Federatioin (2019008), Scientific research project of Zhongyuan University of Technology (K2019YY001), Youth Backbone Teachers Funding Planning of Zhongyuan University of Technology.

References

1 C. B. Nielsen, S. Holliday, H. Y. Chen, S. J. Cryer and I. McCulloch, *Acc. Chem. Res*., 2015, **48**, 2803−2812.

2 G. Li, W. H. Chang and Y. Yang, *Nat. Rev. Mater*., 2017, **2**, 17043.

3 Q. Wu, D. Zhao, A. M. Schneider, W. Chen and L. Yu, *J. Am. Chem. Soc*., 2016, **138**, 7248−7251.

4 A. Polman, M. Knight, E. C. Garnett, B. Ehrler and W. C. Sinke, *Science*, 2016, **352**, 4424.

5 J. Hou, O. Inganäs, R. H. Friend and F. Gao, *Nat. Mater*., 2018, **17**, 119−128.

6 C. Yan, S. Barlow, Z. Wang, H. Yan, A. K. Y. Jen, S. R. Marder and X. Zhan, *Nat. Rev. Mater*., 2018, **3**, 18003.

7 G. Zhang, J. Zhao, P. C. Y. Chow, K. Jiang, J. Zhang, Z. Zhu, J. Zhang, F. Huang and H. Yan, *Chem. Rev*., 2018, **118**, 3447−3507.

8 L. Meng, Y. Zhang, X. Wan, C. Li, X. Zhang, Y. Wang, X. Ke, Z. Xiao, L. Ding, R. Xia, H. L. Yip, Y. Cao and Y. Chen, *Science*, 2018, **361**, 1094−1098.

9 a) J. Yuan, Y. Zhang, L. Zhou, G. Zhang, H. L. Yip, T. K. Lau, X. Lu, C. Zhu, H. Peng, P. A. Johnson, M. Leclerc, Y. Cao, J. Ulanski, Y. Li and Y. Zou, *Joule*, 2019, **3**, 1140−1151; b) K. Jiang, Q. Wei, J. Yuk L. Lai, Z. Peng, H. K. Kim, J. Yuan, L. Ye, H. Ade, Y. Zou and H. Yan, *Joule*, 2019, **3**, 3020–3033.

10 a) J. Yuan, Y. Zhang, L. Zhou, C. Zhang, T. K. Lau, G. Zhang, X. Lu, H. L. Yip, S. K. So, S. Beaupré, M. Mainville, P. A. Johnson, M. Leclerc, H. Chen, H. Peng, Y. Li and Y. Zou, *Adv. Mater*., 2019, **31**, 1807577; b) Y. Wu, Y. Zheng, H. Yang, C. Sun, Y. Dong, C. Cui, H. Yan and Y. Li, *Sci China Chem*., 2019, **62**, DOI: 10.1007/s11426-019-9599-1.

11 B. Fan, D. Zhang, M. Li, W. Zhong, Z. Zeng, L. Ying, F. Huang and Y. Cao, *Sci. China Chem*., 2019, **62**, 746−752.

12 J. Yuan, T. Huang, P. Cheng, Y. Zou, H. Zhang, J. L. Yang, S.-Y. Chang, Z. Zhang, W. Huang, R. Wang, D. Meng, F. Gao and Y. Yang, *Nat. Commun*., 2019, **10**, 570.

13 a) Y. Cui, H. Yao, J. Zhang, T. Zhang, Y. Wang, L. Hong, K. Xian, B. Xu, S. Zhang, J. Peng, Z. Wei, F. Gao and J. Hou, *Nat. Commun*., 2019, **10**, 2515; b) Q. Liao, Q. Kang, Y. Yang, C. An, B. Xu and J. Hou, *Adv. Mater*., 2019, 1906557; c) R. Yu, H. Yao, Y. Cui, L. Hong, C. He and J. Hou, *Adv. Mater*., 2019, 1902302; d) L. Ma, Y. X, Y. Zu, Q. Liao, B. Xu, C. An, S. Zhang and J. Hou, *Sci. China Chem*., 2019, **62**, DOI:10.1007/s11426-019-9556-7.

14 X. Xu, K. Feng, Z. Bi, W. Ma, G. Zhang and Q. Peng, *Adv. Mater*., 2019, **31**, 1901872.

15 Q. An, X. Ma, J. Gao and F. Zhang, *Sci. Bull*., 2019, **64**, 504–506.

16 a) L. Ye, S. Li, X. Liu, S. Zhang, M. Ghasemi, Y. Xiong, J. Hou and H. Ade, *Joule*, 2019, **3**, 443–458; b) L. Ye, H. Hu, M. Ghasemi, T. Wang, B. A. Collins, J.-H. Kim, K. Jiang, J. H. Carpenter, H. Li, Z. Li, T. McAfee, J. Zhao, X. Chen, J. L. Y. Lai, T. Ma, J.-L. Bredas, H. Yan and H. Ade, *Nat. Mater*., 2018, **17**, 253–260.

17 b) L. Hong, H. Yao, Z. Wu, Y. Cui, T. Zhang, Y. Xu, R. Yu, Q. Liao, B. Gao, K. Xian, H. Y. Woo, Z. Ge and J. Hou, *Adv. Mater*., 2019, **31**, 1903441; b) T. Yan, W. Song, J. Huang, R. Peng, L. Huang and Z. Ge, *Adv. Mater*., 2019, **31**, 1902210; c) J. Ge, L. Xie, R. Peng, B. Fanady, J. Huang, W. Song, T. Yan, W. Zhang and Z. Ge, *Angew. Chem. Int. Ed*., 2019, DOI: 10.1002/ange.201910297.

18 a) Y. Chang, T.-K. Lau, M.-A. Pan, X. Lu, H. Yan and C. Zhan, *Mater. Horiz*., 2019, **6**, 2094−2102; b) K. Li, Y. Wu, Y. Tang, M.-A. Pan, W. Ma, H. Fu, C. Zhan and J. Yao, *Adv. Energy Mater*., 2019, **9**, 1901728; c) M. Pan, T. Lau, Y. Tang, Y. Wu, T. Liu, K. Li, M. M. Chen, X. Lu, W. Ma and C. Zhan, *J. Mater. Chem. A*, 2019, **7**, 20713−20722.

19 a) Z. Zhou, W. Liu, G. Zhou, M. Zhang, D. Qian, J. Zhang, S. Chen, S. Xu, C. Yang, F. Gao, H. Zhu, F. Liu and X. Zhu, *Adv. Mater*., 2019, 1906324; b) X. Che, Y. Li, Y. Qu and S. R. Forrest, *Nat. Energy*, 2018, **3**, 422–427; c) Q. Fan, Q. Zhu, Z. Xu, W. Su, J. Chen, J. Wu, X. Guo, W. Ma, M. Zhang and Y. Li, *Nano Energy*, 2018, **48**, 413–420.

20 a) Y. Lin, J. Wang, Z.-G. Zhang, H. Bai, Y. Li, D. Zhu and X. Zhan, *Adv. Mater*., 2015, **27**, 1170–1174; b) Y. Lin, Q. He, F. Zhao, L. Huo, J. Mai, X. Lu, C.-J. Su, T. Li, J. Wang, J. Zhu, Y. Sun, C. Wang and X. Zhan, *J. Am. Chem. Soc*., 2016, **138**, 2973–2976; c) Y. Z. Lin, F. Zhao, Y. Wu, K. Chen, Y. Xia, G. Li, J. Zhu, L. Huo, H. Bin, Z.-G. Zhang, X. Guo, M. Zhang, Y. Sun, F. Gao, Z. Wei, W. Ma, C. Wang, Z. Bo, O. Inganäs, Y. Li and X. Zhan, *Adv. Mater*., 2016, **29**, 1604155.

21 a) W. Zhao, S. Li, H. Yao, S. Zhang, Y. Zhang, B. Yang and J. Hou, *J. Am. Chem. Soc*., 2017, **139**, 7148–7151; b) S. S. Li, L. Ye, W. Zhao, S. Zhang, S. Mukherjee, H. Ade and J. Hou, *Adv. Mater*., 2016, **28**, 9423–9429.

22 a) L. Ye, S. Zhang, L. Huo, M. Zhang and J. Hou, *Acc. Chem. Res*., 2014, **47**, 1595–1603; b) S. Li, L. Ye, W. Zhao, H. Yan, B. Yang, D. Liu, W. Li, H. Ade and J. Hou, *J. Am. Chem. Soc*., 2018, **140**, 7159–7167.

23 L. Lu, T. Zheng, Q. Wu, A. M. Schneider, D. Zhao and L. Yu, *Chem. Rev*., 2015, **115**, 12666–12731.

24 a) Y. Li, *Acc. Chem. Res*., 2012, **45**, 723–733; b) X. Li, F. Pan, C. Sun, M. Zhang, Z. Wang, J. Du, J. Wang, M. Xiao, L. Xue, Z. Zhang, C. Zhang, F. Liu and Y. Li, *Nat. Commun*., 2019, **10**, 519.

25 Q. Zhang, M. A. Kelly, N. Bauer and W. You, *Acc. Chem. Res*., 2017, **50**, 2401–2409.

26 G. Zhang, J. Zhao, P. C. Y. Chow, K. Jiang, J. Zhang, Z. Zhu, J. Zhang, F. Huang and H. Yan, *Chem. Rev*., 2018, **118**, 3447–3507.

27 a) Y. Sun, H.-H. Gao, Y.-Q.-Q. Yi, X. Wan, H. Feng, X. Ke, Y. Zhang, J. Yan, C. Li and Y. Chen, *Sci. China Mater*., 2019, **62**, 1210–1217; b) B. Kan, H. Feng, H. Yao, M. Chang, X. Wan, C. Li, J. Hou and Y. Chen, *Sci. China Mater*., 2018, **61**, 1307−1313.

28 a) Q. Fan, W. Su, Y. Wang, B. Guo, Y. Jiang, X. Guo, F. Liu, T. P. Russell, M. Zhang and Y. Li, *Sci. China Chem*., 2018, **61**, 531−537; b) M. Zhang, Y. Gu, X. Guo, F. Liu, S. Zhang, L. Huo, T. P. Russell and J. Hou, *Adv. Mater*., 2013, **25**, 4944−4949; c) M. Zhang, X. Guo, W. Ma, H. Ade and J. Hou, *Adv. Mater*., 2015, **27**, 4655−4660; d) B. Guo, W. Li, X. Guo, X. Meng, W. Ma, M. Zhang and Y. Li, *Adv. Mater*., 2017, **29**, 1702291.

29 J. Mei and Z. Bao, *Chem. Mater*., 2014, **26**, 604−615.

30 Z. Zhang and Y. Li, *Sci. China Chem*., 2015, **58**, 192−209.

31 S.-H. Liao, H.-J. Jhuo, Y.-S. Cheng and S.-A. Chen, *Adv. Mater*., 2013, **25**, 4766−4771.

32 M. Zhang, X. Guo, S. Zhang and J. Hou, *Adv. Mater*., 2014, **26**, 1118−1123.

33 M. Zhang, X. Guo, W. Ma, S. Zhang, L. Huo, H. Ade and J. Hou, *Adv. Mater*., 2014, **26**, 2089−2095.

34 W. Li, G. Li, X. Guo, B. Guo, Z. Bi, H. Guo, W. Ma, X. Ou, M. Zhang and Y. Li, *J. Mater. Chem. A*, 2017, **5**, 19680−19686.

35 C. Cabanetos, A. E. Labban, J. A. Bartelt, J. D. Douglas, W. R. Mateker, J. M. J. Frechet, M. D. McGehee and P. M. Beaujuge, *J. Am. Chem. Soc*., 2013, **135**, 4656−4659.

36 J. M. Szarko, J. Guo, Y. Liang, B. Lee, B. S. Rolczynski, J. Strzalka, T. Xu, S. Loser, T. J. Marks, L. Yu and L. X. Chen, *Adv. Mater*., 2010, **22**, 5468−5472.

37 J. Yao, C. Yu, Z. Liu, H. Luo, Y. Yang, G. Zhang and D. Zhang, *J. Am. Chem. Soc*., 2016, **138**, 173−185.

38 a) T. Lei, J.-H. Dou, J. Pei, *Adv. Mater.* 2012, **24**, 6457−6461; b) I. Osaka, M. Saito, T. Koganezawa and K. Takimiya, *Adv. Mater*., 2014, **26**, 331−338.

39 L. Yang, J. R. Tumbleston, H. Zhou, H. Ade and W. You, *Energy Environ. Sci*., 2013, **6**, 316−326.

40 Y. Liu, J. Zhao, Z. Li, C. Mu, W. Ma, H. Hu, K. Jiang, H. Lin, H. Ade and H. Yan, *Nat. Commun*., 2014, **5**, 5293.

41 a) H. Bin, L. Gao, Z.-G. Zhang, Y. Yang, Y. Zhang, C. Zhang, S. Chen, L. Xue, C. Yang, M. Xiao and Y. Li, *Nat. Commun*., 2016, **7**, 13651; b) Y. Yang, Z.-G. Zhang, H. Bin, S. Chen, L. Gao, L. Xue, C. Yang and Y. Li, *J. Am. Chem. Soc*., 2016, **138**, 15011−15018.

42 T. Liu, X. Pan, X. Meng, Y. Liu, D. Wei, W. Ma, L. Huo, X. Sun, T. H. Lee, M. Huang, H. Choi, J. Y. Kim, W. C. H. Choy and Y. Sun, *Adv. Mater*., 2017, **29**, 1604251.

43 Q. Fan, W. Su, X. Guo, Y. Wang, J. Chen, C. Ye, M. Zhang and Y. Li, *J. Mater. Chem. A*, 2017, **5**, 9204−9029.

44 H. Bin, Z.-G. Zhang, L. Gao, S. Chen, L. Zhong, L. Xue, C. Yang and Y. Li, *J. Am. Chem. Soc*., 2016, **138**, 4657−4664.

45 Y. Dong, X. Hu, C. Duan, P. Liu, S. Liu, L. Lan, D. Chen, L. Ying, S. Su, X. Gong, F. Huang and Y. Cao, *Adv. Mater*., 2013, **25**, 3683−3688.

46 D. Liu, C. Gu, J. Wang, D. Zhu, Y. Li, X. Bao and R. Yang, *J. Mater. Chem. A*, 2017, **5**, 9141−9147.

47 L. Huo, T. Liu, B. Fan, Z. Zhao, X. Sun, D. Wei, M. Yu, Y. Liu and Y. Sun, *Adv. Mater*., 2015, **27**, 6969−6975.

48 X. Guo, M. Zhang, J. Tan, S. Zhang, L. Huo, W. Hu, Y. Li and J. Hou, *Adv. Mater*., 2012, **24**, 6536−6541.

49 W. Li, B. Guo, C. M. Chang, X. Guo, M. Zhang and Y. Li, *J. Mater. Chem. A*, 2016, **4**, 10135−10141.

50 W. Su, Q. Fan, X. Guo, B. Guo, W. Li, Y. Zhang, M. Zhang and Y. Li, *J. Mater. Chem. A*, 2016, **4**, 14752−14760.

51 J.-L. Wu, F.-C. Chen, Y.-S. Hsiao, F.-C. Chien, P. Chen, C.-H. Kuo, M. H. Huang and C.-S. Hsu, *ACS Nano*, 2011, **5**, 959−967.

52 P. W. Blom, V. D. Mihailetchi, L. J. Koster and D. E. Markov, *Adv. Mater*., 2007, **19**, 1551−1566.

53 M. Lenes, M. Morana, C. J. Brabec and P. W. M. Blom, *Adv. Funct. Mater*., 2009, **19**, 1106−1111.